Amplitude modulation of quantum-ion-acoustic wavepackets in electron-positron-ion plasmas: Modulational instability, envelope modes, extreme waves[a)]

Ata-ur-Rahman,[1,2,b)] Michael Mc Kerr,[3,c)] Wael F. El-Taibany,[4,5,d)] Ioannis Kourakis,[3,e)] and A. Qamar[1,f)]
[1]*Department of Physics, University of Peshawar, Peshawar 25000, Pakistan*
[2]*Department of Physics, Islamia College Peshawar, Khyber Pakhtunkhwa, Pakistan*
[3]*Centre for Plasma Physics, Department of Physics and Astronomy, Queen's University Belfast, BT7 1NN Northern Ireland, United Kingdom*
[4]*Department of Physics, Faculty of Science, Damietta University, New Damietta, P.O. Box 34517, Egypt*
[5]*Department of Physics, College of Science for Girls in Abha, King Khalid University, P.O. Box 960, Abha, Saudi Arabia*

(Received 26 August 2014; accepted 21 January 2015; published online 11 February 2015)

A semirelativistic fluid model is employed to describe the nonlinear amplitude modulation of low-frequency (ionic scale) electrostatic waves in an unmagnetized electron-positron-ion plasma. Electrons and positrons are assumed to be degenerated and inertialess, whereas ions are warm and classical. A multiscale perturbation method is used to derive a nonlinear Schrödinger equation for the envelope amplitude, based on which the occurrence of modulational instability is investigated in detail. Various types of localized ion acoustic excitations are shown to exist, in the form of either bright type envelope solitons (envelope pulses) or dark-type envelope solitons (voids, holes). The plasma configurational parameters (namely, the relativistic degeneracy parameter, the positron concentration, and the ionic temperature) are shown to affect the conditions for modulational instability significantly, in fact modifying the associated threshold as well as the instability growth rate. In particular, the relativistic degeneracy parameter leads to an enhancement of the modulational instability mechanism. Furthermore, the effect of different relevant plasma parameters on the characteristics (amplitude, width) of these envelope solitary structures is also presented in detail. Finally, the occurrence of extreme amplitude excitation (rogue waves) is also discussed briefly. Our results aim at elucidating the formation and dynamics of nonlinear electrostatic excitations in superdense astrophysical regimes. © *2015 AIP Publishing LLC*. [http://dx.doi.org/10.1063/1.4907247]

I. INTRODUCTION

The nonlinear characteristics of electrostatic waves in quantum (degenerate) plasmas form a subject of increasing interest nowadays. Such plasmas exist in dense astrophysical environments (e.g., in white and brown dwarf stars, in neutron stars, etc.), in the cores of some giant planets and, interestingly, also in the laboratory (e.g., in super-intense laser-dense matter experiments).[1–5] In dense astrophysical environments and in superdense laser-produced plasmas, physical parameters like density, magnetic field, and temperature may vary over a wide range of values. For example, in white dwarfs, the electron number density is extremely high[4,6] (typically $10^{30}\,\mathrm{cm}^{-3}$ or higher). Quantum and/or relativistic effects inevitably become relevant in such situations, as the inter-electron distance becomes comparable to, or less than, the thermal de Broglie wavelength $\lambda_B = h/m_e v_{Te}$ (where h is Planck's constant, m_e is the electron mass, and v_{Te} is electron thermal speed). Quantum effects are more prominent for lighter species (electrons), compared to heavier species (ions), whose behavior may be quasi-classical, depending on the degeneracy parameter $n\lambda_B^3$, where n is the plasma number density (recall that $n\lambda_B^3 \gg 1$ for quantum plasmas to be treated as such). Moreover, in extremely high densities, the electron Fermi energy E_F can be much higher than the thermal energy ($\sim k_B T$). The thermal pressure of electrons can thus be ignored, compared to the Fermi degeneracy pressure, which arises due to the Pauli exclusion principle. Under such extreme conditions, the equation of state for the degeneracy pressure of electrons also changes from $P \sim n^{5/3}$ (non-relativistic case) to $P \sim n^{4/3}$ (ultra-relativistic case).[1,7] This degenerate electron pressure, which depends on the density but not on the temperature, is what supports dense astrophysical objects (e.g., white dwarfs) against the tremendous gravitational forces that would otherwise cause the object to collapse.

Extensive research has been carried out recently to understand the essential physics and basic features of relativistic degenerate plasmas. Mamun and Shukla[8] studied small-amplitude solitary waves by assuming ultra-relativistic degenerate electrons and cold ions, via a Korteweg-de Vries (KdV) theory. Their work was later extended to electron-positron-ion (e-p-i) plasmas,[9] consisting of ultra-relativistic degenerate electrons and positrons

[a)]Work carried out during a research visit to: Centre for Plasma Physics, Department of Physics and Astronomy, Queen's University Belfast, BT7 1NN Northern Ireland, United Kingdom.
[b)]Email: ata797@yahoo.com
[c)]Email: mjamckerr@gmail.com
[d)]Email: eltaibany@hotmail.com
[e)]Email: IoannisKourakisSci@gmail.com
[f)]Email: anisaqamar@gmail.com

and warm, non-degenerate ions. They investigated both weak- and large-amplitude ion-acoustic solitary waves (pulses) and discussed their dependence on various plasma parameters, suggesting a relevance of their work to white dwarfs and to magnetar coronas. An investigation of arbitrary-amplitude ion waves with relativistic degenerate electrons in a wide range of values of the relativity parameter $p_{Fe}/m_e c$ (degree of electron degeneracy) was carried out for the first time by Akbari-Moghanjoughi.[10]

Electron positron (e-p) plasmas are believed to exist in many astrophysical environments (see, e.g., Refs. 11–15), and are also thought to have played an important role in the beginning and evolution of the universe.[16] The dynamics of e-p plasmas has also stirred a great deal of interest in recent years, due to their realization in the laboratory by intense-laser matter interaction experiments.[17–19] In dense astrophysical plasmas where *e-p* plasmas are dominant, ions may also be present,[20] thus, modifying the response of *e-p* plasmas. With a positron lifetime of sufficient duration, the physical system of relevance is essentially a three-component e-p-i plasma. Quantum effects of electrons and positrons in superdense e-p-i plasmas cannot be ignored. It is also interesting to mention here that in relativistic degenerate e-p-i plasmas, the characteristic nonlinear wave frequency is much higher than that of the pair annihilation mechanism (i.e., $\omega_{p,j}^{-1} \ll \tau_{ann}$), therefore it is of practical interest to study waves and nonlinear structures in such a plasma.[21,24] In particular for relativistic degenerate plasmas the annihilation time τ_{ann} is $\tau_{ann} = \frac{4\Theta^2}{3n_j\sigma_\tau c}/[1/4 + \ln(2\delta\Theta + 1)]$ for $\Theta \gg 1$, where $\sigma_\tau (= 6.65 \times 10^{-25}\,\mathrm{cm}^2)$ is the electron Thomson cross-section, $\Theta (= k_B T_{Fj}/m_j c^2)$ is the normalized thermal energy and $\delta = e^{-\Xi_E} \equiv 0.5615$ with $\Xi_E (\approx 0.5772)$ the Euler's constant. By employing $n_{e0} = n_{p0} = n_0$, the pair annihilation condition becomes $(\Theta^2/[1/4 + \ln(1.123\Theta + 1)]) \gg 2.6 \times 10^{-19} n_0^{1/2}$, which is well satisfied for the typical mass density range $\rho \sim 10^6$ g/cm^{-3} characteristic of relativistic dense plasmas found in astrophysical environments (viz., white dwarfs, etc.). Various studies of linear and nonlinear waves in relativistic degenerate e-p-i plasmas have appeared in recent years.[9,22–26]

The study at hand focuses in particular, on modulational instability (MI), one of the most intriguing mechanisms in plasma physics, involving the amplitude modulation of a wavepacket, an evolutionary stage often associated with the formation of localized pulses. Such pulses are efficiently modeled as envelope solitons (so called due to their envelope structure, modulating an internal carrier wave), which are exact solutions of the integrable nonlinear Schrödinger equation (NLSE), successfully modeling the balance between nonlinearity and wave group dispersion. In plasmas, the NLSE can be derived by employing a multiple (space- and time-) scales perturbation technique.[27,28] MI has been subject of extensive investigation in recent years, and its occurrence has been investigated with respect to various wave modes in dispersive and nonlinear plasmas. In 1977, Watanabe reported the first experimental observation of the MI of a monochromatic ion acoustic wave.[29] Subsequently, a number of theoretical investigations focused on the effect(s) of finite ion temperature,[30,31] modulation obliqueness,[33] charged dust,[32,33] nonthermal electrons,[36] positron concentration,[37] among other factors, on the MI characteristics of electrostatic plasma waves.

Our aim is to investigate the nonlinear dynamics of modulated electrostatic ion acoustic wavepackets in ultrahigh density (degenerate) quantum plasmas. We consider an unmagnetized dense plasma composed of inertial non-degenerate warm ions and inertialess relativistic degenerate electrons and positrons. We investigate the occurrence of MI as well as the existence of envelope-type solitary structures associated with ion acoustic waves. The layout of the article goes as follows. In Sec. II, we present a semirelativistic fluid model for ion acoustic waves. In Sec. III, we apply a multiscale perturbation technique, and proceed by discussing the linear behavior of ion acoustic waves and subsequently deriving a NLSE-type equation governing the nonlinear dynamics of ion acoustic waves. In Sec. IV, we derive a nonlinear dispersion relation for a long-wavelength "random" perturbation of the modulated amplitude. In Sec. V, we summarize the basic information on relevant envelope soliton solutions of the NLSE. Breather-type rogue-wave-like solutions are presented in Sec. VI. Sec. VII is devoted to a parametric investigation in terms of different relevant parameters, while Sec. VIII is dedicated to the conclusion of our results.

II. QUANTUM ION-FLUID MODEL

We are interested in modeling electrostatic excitations at the ionic frequency scale propagating in an unmagnetized e-p-i plasma. For simplicity, we adopt a one-dimensional geometry. The ions are assumed to constitute a non-degenerate system of particles with an individual charge of $Z_i e$ (where Z_i denotes the ion charge state, and e is the electron charge). Self-induced electric forces occur, due to variations of an electrostatic potential ϕ, while the electrons and positrons obey Fermi-Dirac statistics and are considered a relativistically degenerate ensemble. Adopting a one-dimensional semiclassical fluid formulation, the evolution equations for the ion density n_i, fluid speed v_i and electron/positron pressure $P_{e/p}$, in terms of ϕ, read

$$\begin{aligned}
&\frac{\partial n_i}{\partial t} + \frac{\partial}{\partial x}(n_i v_i) = 0,\\
&\frac{\partial v_i}{\partial t} + v_i\frac{\partial v_i}{\partial x} + \frac{Z_i e}{m_i}\frac{\partial \phi}{\partial x} + \frac{1}{m_i n_i}\frac{\partial P_i}{\partial x} = 0,\\
&e n_e \frac{\partial \phi}{\partial x} - \frac{\partial P_e}{\partial x} = 0,\\
&e n_p \frac{\partial \phi}{\partial x} + \frac{\partial P_p}{\partial x} = 0,\\
&\frac{\partial^2 \phi}{\partial x^2} = 4\pi e(n_e - Z_i n_i - n_p).
\end{aligned} \tag{1}$$

Electrons and positrons are treated as a degenerate ensemble, following the equation(s) of state

$$P_j = \frac{\pi m_j^4 c^5}{3h^3}\left[\eta_j\left(2\eta_j^2 - 3\right)\left(1 + \eta_j^2\right)^{\frac{1}{2}} + 3\sinh^{-1}(\eta_j)\right], \tag{2}$$

where $\eta_j = p_{Fj}/m_j c = \sqrt{\gamma_j^2 - 1}$ and $p_{Fj} = (3h^3 n_j/8\pi)^{\frac{1}{3}}$; the index j will denote either electrons (e) or positrons (p) throughout this text.

The third and fourth equations in system (1) above are readily eliminated by employing the expression: $\frac{1}{n_j}\frac{\partial P_j}{\partial x} = \frac{m_j c^2 \eta_j}{(1+\eta_j^2)^{\frac{1}{2}}}\frac{\partial \eta_j}{\partial x}$ and then integrating to find a relation between n_j and ϕ in the form

$$n_{e,p} = \frac{8\pi m_{e,p}^3 c^3}{3h^3}\left[\frac{e^2\phi^2}{m_{e,p}^2 c^4} \pm \frac{2e\phi}{m_{e,p}c^2}\left(1+\eta_{e,p0}^2\right)^{\frac{1}{2}} + \eta_{e,p0}^2\right]^{\frac{3}{2}}. \quad (3)$$

In (3), $\eta_{j0} = (3h^3 n_{j0}/8\pi m_j^3 c^3)^{1/3}$ is the value of the relativity parameter, η_j, at equilibrium.

A. Scaled evolution equations

The model may be rewritten in terms of dimensionless variables. Number densities have been rescaled by their equilibrium values. Here, we adopt a natural choice of scales: time and space are, respectively, scaled by the inverse plasma frequency $\omega_{pi}^{-1} = (m_i/4\pi n_{i0} Z_i^2 e^2)^{1/2}$ and by the characteristic length C_i/ω_{pi}, where the ion fluid speed is scaled over $C_i = (E_{Fe0}/m_i)^{1/2}$. The electrostatic potential is scaled by $E_{Fe0}/Z_i e$.

Applying the above scale transformation, one obtains

$$\begin{aligned}
&\frac{\partial \tilde{n}_i}{\partial \tilde{t}} + \frac{\partial}{\partial \tilde{x}}(\tilde{n}_i \tilde{v}_i) = 0,\\
&\frac{\partial \tilde{v}_i}{\partial \tilde{t}} + \tilde{v}\frac{\partial \tilde{v}_i}{\partial \tilde{x}} + \frac{\partial \tilde{\phi}}{\partial \tilde{x}} + g\tilde{n}_i\frac{\partial \tilde{n}_i}{\partial \tilde{x}} = 0,\\
&\frac{\partial^2 \tilde{\phi}}{\partial \tilde{x}^2} = \beta\tilde{n}_e - \tilde{n}_i - \alpha\tilde{n}_p,
\end{aligned} \quad (4)$$

where all quantities are dimensionless (real numbers).

We have defined the dimensionless parameters: $\alpha = \frac{n_{p0}}{|Z_i|n_{i0}}$ and $\beta = \frac{n_{e0}}{|Z_i|n_{i0}}$. Overall charge neutrality at equilibrium imposes a balance relation on the plasma components' number densities, leading to the constraint: $\beta = \alpha + 1$. This relation can be used to express the electron equilibrium density (and, subsequently, the positron equilibrium Fermi energy) in terms of that of the positrons, once the value of α is fixed.

We have also defined the ratio $g = 3\frac{T_i}{T_{Fe0}}$, measuring the relative strength between the ion temperature (T_i) and the electron Fermi temperature ($T_{Fe0} = E_{Fe0}/k_B$, where k_B is the Boltzmann constant, in principle a very small number).

Assuming excitations not too far from equilibrium, Poisson's equation can be expanded in a Taylor series in the electrostatic potential, viz.,

$$\frac{\partial^2 \tilde{\phi}}{\partial \tilde{x}^2} + \tilde{n}_i - 1 \approx c_1\tilde{\phi} + c_2\tilde{\phi}^2 + c_3\tilde{\phi}^3, \quad (5)$$

where we have defined the expansion coefficients

$$\begin{aligned}
c_1 &= \frac{3}{2Z_i}\left[(1+\alpha)\gamma_{e0} + \alpha\gamma_{p0}\frac{E_{F,e0}}{E_{F,p0}}\right],\\
c_2 &= \frac{3}{8Z_i^2}\left[(1+\alpha)\left(2\gamma_{e0}^2 - 1\right) - \alpha\left(2\gamma_{p0}^2 - 1\right)\left(\frac{E_{F,e0}}{E_{F,p0}}\right)^2\right],\\
c_3 &= \frac{1}{16Z_i^3}\left[(1+\alpha)\gamma_{e0}\left(2\gamma_{e0}^2 - 3\right),\right.\\
&\quad \left. +\alpha\gamma_{p0}\left(2\gamma_{p0}^2 - 3\right)\left(\frac{E_{F,e0}}{E_{F,p0}}\right)^3\right].
\end{aligned} \quad (6)$$

It is appropriate to express the relativistic degeneracy parameter for positrons, η_{p0}, in terms of the electron relativistic degeneracy parameter, η_{e0}. In this case, $\eta_{p0} = (\alpha/\beta)^{1/3}\eta_{e0}$, where $\eta_{e0} = (3/8\pi)^{1/3}(h/m_e c)n_{e0}^{1/3}$ measures the relativistic degeneracy effects. The subscript "0" in γ_{e0} (γ_{p0}) indicates that the electron (positron) density is to be evaluated at equilibrium and $E_{Fj0} = m_j c^2 \eta_{j0}^2/2$. We shall later show that c_1 is related to the shielding length in the plasma considered, and is in fact present in the first-order (linear) response, whereas c_2 and c_3 appear only at higher orders in the expansion, and are associated with the intrinsic nonlinearity of the physical problem.

For the remainder of this work, the tilde over the dimensionless variables in the system (4) will be dropped.

The above choice of scales, which is common and physically transparent, for dense plasmas greatly simplifies the analytical work. However, we should point out, for rigor, that there is extra dependence on the density hidden from sight within the scaling and this might arguably affect some of the plots. Therefore, the plots presented in the following have been made with respect to different (fixed) scales, which are not density dependent: for this purpose, we have introduced two constants, $\omega_0 = 8\pi(m_e^3 c^3/6m_i h^3)^{1/2}\mathrm{s}^{-1}$ and $k_0 = 8\pi m_e e(c/3h^3)^{1/2}\,\mathrm{cm}^{-1}$, which will be used later in the plots.

III. MULTIPLE SCALES PERTURBATION

We consider each of n_i, v_i and ϕ as a modulated envelope, i.e., the convolution of a fast internal (carrier) wave with a slowly varying amplitude. It is assumed that the carrier depends only on the fast $\{x,t\} \equiv \{X_0, T_0\}$ scale, while the slowly evolving envelope depends on an infinite set of slow scales, $\{X_1, X_2, ..., T_1, T_2, ...\}$, where the different scales $T_r = \epsilon^r t$ and $X_r = \epsilon^r x$ (for $r = 1, 2, 3, ...$) are introduced, and $\epsilon \ll 1$ is a free (real, small) parameter. Near equilibrium, the variables are expanded as $n_i \approx 1 + \epsilon n_{i1} + \epsilon^2 n_{i2} + \cdots$, $v_i \approx \epsilon v_{i1} + \epsilon^2 v_{i2} + \cdots$, and $\phi \approx \epsilon\phi_1 + \epsilon^2\phi_2 + \cdots$, while each of these contributions u_j (say, any of n_j, v_j, ϕ_j) is split into a sum of Fourier components: $u_j = \sum_{r=-j}^{j} u_j^{(r)} e^{ir(kx-\omega t)}$. The number density and fluid speed of each species, and also the electrostatic potential are real-valued quantities, so $u_j^{(-r)} = \bar{u}_j^{(r)}$ (the bar here denoting the complex conjugate). The stretched variables are treated as independent variables. With this in mind, the model equations are transformed into a series of coupled polynomials whose solutions provide expressions for the state variables in terms of their harmonic amplitudes.

A. Linear analysis

The compatibility of the system obtained to first-order in the expansion parameter ϵ leads to the linear dispersion relation

$$\omega^2 = \frac{k^2}{c_1 + k^2} + gk^2. \quad (7)$$

The dispersion characteristics of the carrier wave are depicted in Figures 1 and 2.

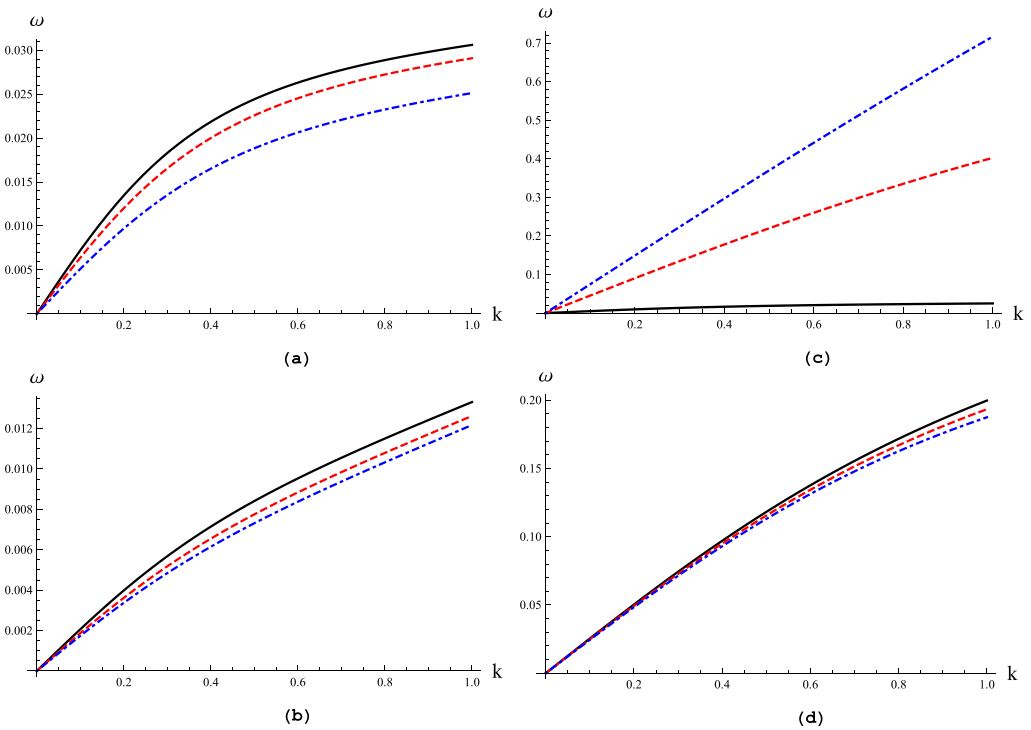

FIG. 1. The (angular) wave frequency ω (in units of $\omega_0 = 8\pi(m_e^3c^3/6m_ih^3)^{1/2}$) is plotted against k (in units of $k_0 = 8\pi m_e e(c/3h^3)^{1/2}$). In (a), $\eta_{e0} = 10g = 0.1$ and the solid/dashed/dotted-dashed curves represent $\alpha = 0.01/0.1/0.5$. In (b), $\eta_{e0} = 10g = 0.1$ and the solid/dashed/dotted-dashed curves represent $\alpha = 1/9/15$. In (c), $\alpha = 50g = 0.5$ and the solid/dashed/dotted-dashed curves represent $\eta_{e0} = 0.1/1/2$. In (d), $\eta_{e0} = \alpha = 0.5$ and the solid/dashed/dotted-dashed curves represent $g = 0.02/0.01/0.001$.

The first order perturbation amplitudes (ϕ_1, n_{i1} and v_{i1}) are obtained, in terms of the first-order electric potential correction (amplitude) $\phi_1^{(1)} = \psi$ (undetermined, a free variable) as $\phi_1 = \psi\, e^{i(kx-\omega t)} + \bar{\psi}\, e^{-i(kx-\omega t)}$ and $v_{i1}^{(1)} = \frac{\omega}{k} n_{i1}^{(1)} = \frac{\omega}{k}(c_1 + k^2)\psi$.

B. Nonlinear analysis and the nonlinear Schrödinger equation

The equations for the first-harmonic components at second order are singular, unless the secular terms are annihilated. This leads to the following requirement:

$$\frac{\partial \psi}{\partial T_1} + v_g \frac{\partial \psi}{\partial X_1} = 0, \tag{8}$$

where $v_g = d\omega/dk = [c_1/(c_1 + k^2)^2 + g]k/\omega$. This condition suggests that the envelope moves at the group velocity, thus $\psi = \psi(X_1 - v_g T_1)$.

In the next (second) order in ϵ, one obtains a set of expressions for the first-, second-, and zeroth-harmonic components, which turn out to be proportional to $\partial\psi/\partial X_1$, ψ^2, and $|\psi|^2$, respectively. We retain, in the following, the formal expression for the electrostatic potential:

$$\phi \approx \epsilon\, \psi\, e^{i(kX_0 - \omega T_0)} + \epsilon^2 \left(\frac{1}{2} C_{2_3}^0 |\psi|^2 + C_{2_3}^2 \psi^2 e^{2i(kX_0 - \omega T_0)} \right) + c.c., \tag{9}$$

alongside analogous expressions for the ion density and the ion fluid speed (for details, see the Appendix).

Proceeding to third order in ϵ, annihilation of the secular terms associated with the first harmonics arising in the algebra, require ψ to obey an equation in the form

$$i\frac{\partial \psi}{\partial \tau} + P\frac{\partial^2 \psi}{\partial \xi^2} + Q|\psi|^2\psi = 0, \tag{10}$$

where we have defined the "slow" coordinates $\xi = X_1 - v_g T_1 = \epsilon(x - v_g t)$ and $\tau = T_2 = \epsilon^2 t$.

Due to its structure, the latter partial differential equation is referred to in the literature as the nonlinear Schrödinger equation.[33] The dispersive coefficient, P, is related to the gradient of the group velocity, viz., $P = \frac{1}{2}\frac{dv_g}{dx}$. The nonlinearity coefficient, Q, is given by a lengthy expression, provided in the Appendix.

The dispersion (P) and nonlinearity (Q) coefficients and their product (PQ) are depicted in Figure 3 below, as functions of the carrier wavenumber, for varying values of the relativistic degeneracy parameter η_{e0}. We note that $P < 0 < Q$ near $k \simeq 0$ (i.e., in the long wavelength limit), thus ensuring modulational stability for large wavelengths, as discussed in Sec. IV.

Both coefficients P and Q are functions of the carrier wavenumber k. Let us focus on the large carrier wavelength (small wavenumber) region. A long-wavelength expansion ($k \ll 1$) yields the following approximate expressions:

$$P \approx -\frac{3k}{2c_1^{3/2}\sqrt{1 + c_1 g}}, \qquad Q \approx \frac{Q_0}{k},$$

where

$$Q_0 = \frac{1}{c_1^{3/2}\sqrt{1 + gc_1}} \left(\frac{c_2}{c_1} - \frac{3c_1}{2} - 2gc_1^2 \right) \times \left[\frac{c_2 c_1}{3} - \frac{c_1^3}{6}(3 + 4gc_1) \right]. \tag{11}$$

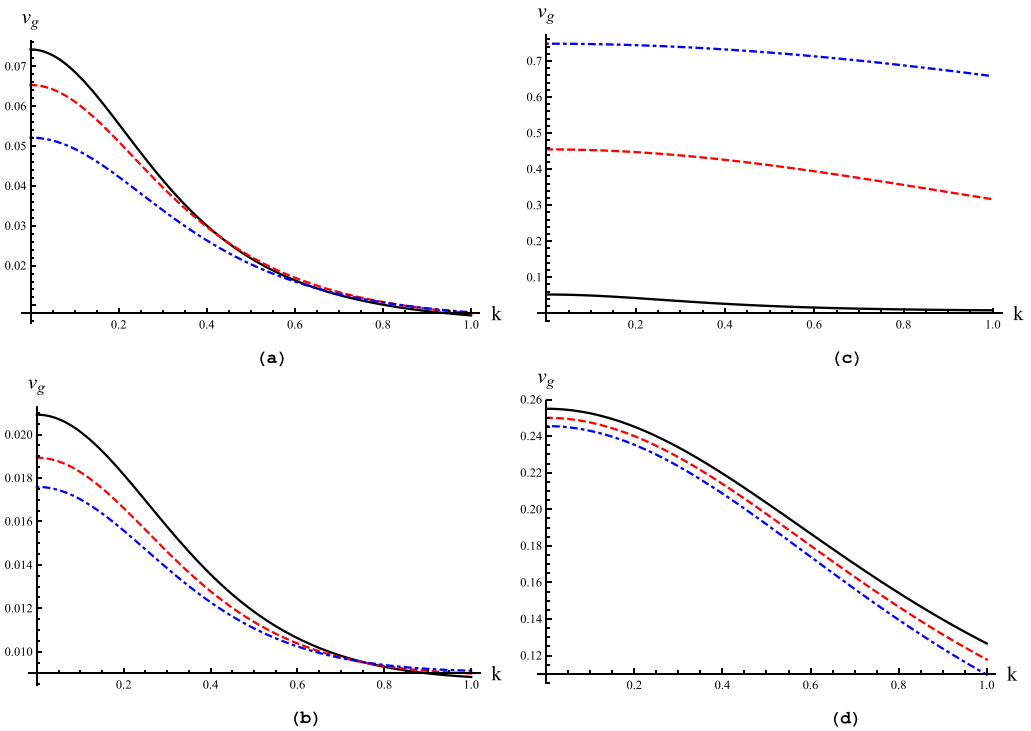

FIG. 2. The group velocity v_g (in units of ω_0/k_0) is plotted against k (in units of k_0). In (a), $\eta_{e0} = 10g = 0.1$ and the solid/dashed/dotted-dashed curves represent $\alpha = 0.01/0.1/0.5$. In (b), $\eta_{e0} = 10g = 0.1$ and the solid/dashed/dotted-dashed curves represent $\alpha = 1/9/15$. In (c), $\alpha = 50g = 0.5$ and the solid/dashed/dotted-dashed curves represent $\eta_{e0} = 0.1/1/2$. In (d), $\eta_{e0} = \alpha = 0.5$ and the solid/dashed/dotted-dashed curves represent $g = 0.02/0.01/0.001$.

The NLSE (10) is the main outcome of the analysis at this stage. The evolution of the wave's amplitude depends on the coefficients P and Q,[33] whose analytical behavior may now be investigated in terms of the physical parameters involved in the problem.

IV. MODULATIONAL INSTABILITY ANALYSIS

Let us here present a brief review for the envelope stability analysis, as described by the NLSE above. We start by defining a monochromatic (Stokes') wave solution[38,39] $\psi_0 = \Psi e^{iQ|\psi|^2\tau}$. We proceed by linearizing around the harmonic solution, viz., $\Psi = \Psi_0 + \varepsilon\Psi_1$, and then taking the perturbation Ψ_1 to be of the form $\Psi_1 = \Psi_{10}\, e^{i(\hat{k}\xi - \hat{\omega}\tau)} + c.c.$, where $c.c.$ denotes the complex conjugate, $\hat{k}$ and $\hat{\omega}$ are the perturbed wave number and the frequency, respectively. Upon substituting into Eq. (10), we obtain the nonlinear dispersion relation

$$\hat{\omega}^2 = P^2\hat{k}^2\left(\hat{k}^2 - 2\frac{Q}{P}|\Psi_{10}|^2\right), \tag{12}$$

relating the (amplitude perturbation) frequency $\hat{\omega}$ and wavenumber $\hat{k}$ (to be distinguished from the carrier frequency ω and wavenumber k).

From the latter relation, we find that the wave is stable for all values of $\hat{k}$ that lead to a negative value for Q/P (recall that Q and P have different signs for small k), however it becomes unstable for wavenumber $\hat{k}$ values that correspond to a positive Q/P, viz., $\hat{k} < \sqrt{2Q/P}|\Psi_{10}|$ (assuming that Q and P have the same sign). This is essentially the well known Benjamin-Feir instability mechanism in hydrodynamics.[38]

V. ENVELOPE EXCITATION MODES

The NLSE (10) possesses different types of solutions, in the form of localized envelope structures (bright or dark), depending on the sign of the product PQ. The different envelope soliton solutions of the NLSE can be found in literature see, e.g., Refs. 34, 35, and 39–41—thus only the main information will be provided in the following text.

In order to obtain stationary-profile localized excitations of the modulated (electrostatic potential) envelope, one may introduce the ansatz[39] $\psi(\xi,\tau) = \Psi(\xi,\tau)\exp[i\Delta(\xi,\tau)]$, where Ψ and Δ are real variables to be determined by substituting into the NLSE (10). Different types of solutions are thus obtained.

When both P and Q have the same sign (i.e., for large wavenumbers—see Figure 3) the carrier wave is modulationally unstable; it may either collapse, due to random external perturbations, or evolve into a series of bright envelope modulated wavepackets, i.e., localized envelope pulses confining the fast carrier wave; for a graphical representation of envelope solitons see, e.g., in Ref. 33. The exact expression for bright-type pulses (occurring only for positive Q/P), as derived rigorously in Ref. 39 (also see Ref. 41), reads

$$|\Psi| = \Psi_m \mathrm{sech}\left(\frac{\xi - V\tau}{L}\right) \quad \text{and}$$
$$\Delta = \frac{1}{2P}\left[V\xi - \left(\frac{1}{2}V^2 + \Omega\right)\tau\right], \tag{13}$$

where Ψ_m is a constant and represents the nonlinear maximum amplitude, and the soliton width is given by $L = (2P/Q)^{1/2}/\Psi_m$. V is the soliton propagation speed and Ω is its frequency at rest. Although the bright envelope soliton phase profile remains constant as it propagates, its phase

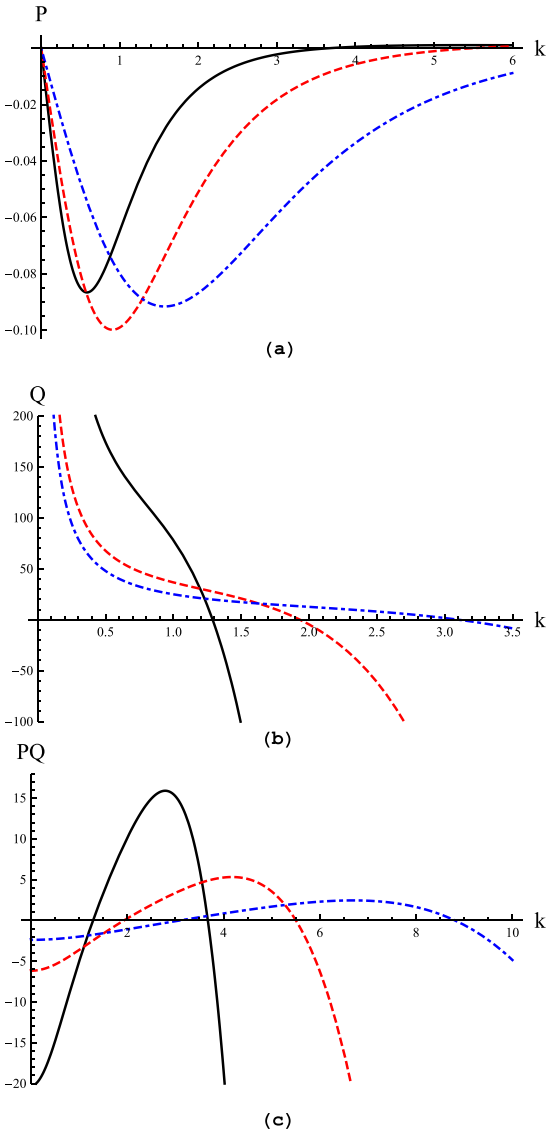

FIG. 3. (a) The dispersion coefficient P (in units of ω_0/k_0^2) is plotted against the wavenumber k (in units of k_0). (b) The nonlinearity coefficient Q (in units of $4\omega_0/m_e^2c^4$) is plotted against the wavenumber k. (c) The product PQ (in units of $4\omega_0^2/m_e^2c^4k_0^2$) plotted against the wavenumber k. In all plots, the solid black curves are for $\eta_{e0} = 0.5$, dashed red curves for $\eta_{e0} = 1$, and dotted-dashed blue curves for $\eta_{e0} = 2$. We have taken $\alpha = 0.5$ and $g = 0.01$.

is characterized by a slow space and time dependence, allowing for a slight deformation of the wave packet internal structure during propagation.

On the other hand, when Q and P have opposite signs (i.e., in the region represented by small wavenumber values—see Figure 3), the wave is modulationally stable and the wavepacket may take the form of a dark (black or grey) envelope wavepacket, i.e., a propagating localized "hole" soliton (see, e.g., Ref. 33). The exact expression for "black" envelopes reads,[39,41]

$$|\Psi| = \Psi_m \tanh\left(\frac{\xi - V\tau}{L_1}\right) \quad \text{and}$$
$$\Delta = \frac{1}{2P}\left[V\xi - \left(\frac{1}{2}V^2 - 2PQ\Psi_m^2\right)\tau\right]. \qquad (14)$$

The dark soliton width L_1 depends on the maximum amplitude Ψ_m via $L_1 = \sqrt{2|P/Q|}/\Psi_m$.

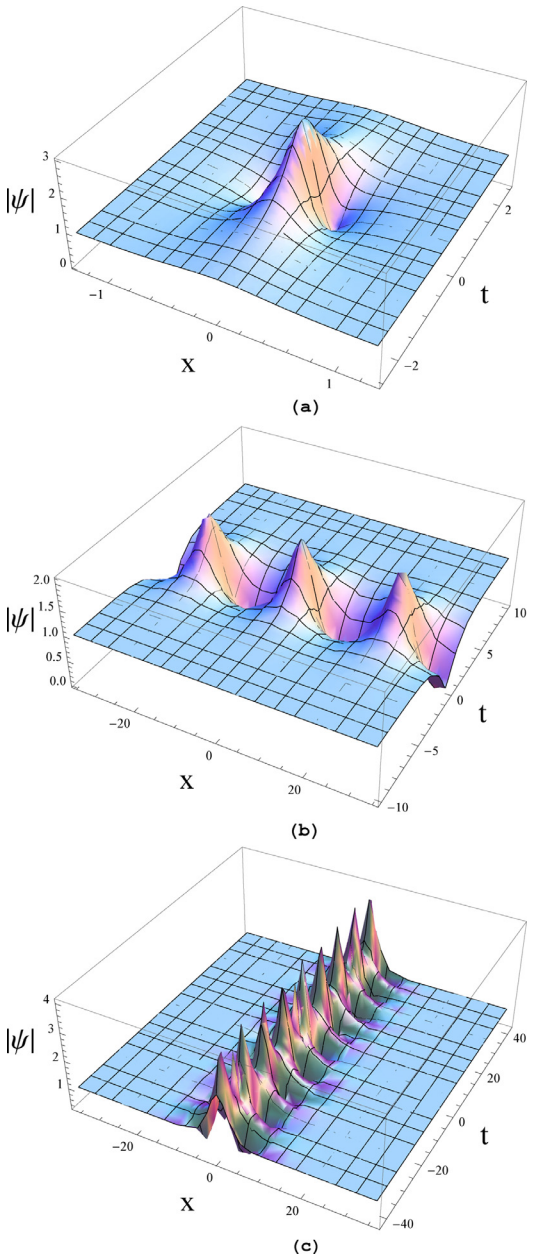

FIG. 4. Plots of (a) Peregrine soliton; (b) Akhmediev breather; (c) the Kuznetsov-Ma breather. We have considered here the values: $\alpha = 0.5$, $\eta_{e0} = 0.01$ and $g = 0.01$.

For more details about the main characteristics of these envelope solitons, the interested reader is referred to Ref. 42 (also see Ref. 33 for a discussion).

VI. BREATHER TYPE SOLUTIONS OF THE NLSE (10) AS MODELS FOR ROGUE WAVES

Rogue waves—also known as freak waves, extreme waves, monster waves, or WANDTs ("waves that appear from nowhere and disappear without a trace")—represent one of the most fascinating natural phenomena frequently observed in mid-ocean and coastal waters.[43] A rogue wave is a short-lived, extreme-amplitude phenomenon which appears in the ocean in an apparently random manner, bearing an amplitude much higher than twice the average wave turbulence level around it.

It was recognized at an early stage that linear theories fail to provide explanation for the formation of rogue waves,[44,45] hence researchers resorted to nonlinear theories[45,46] to explain rogue wave formation. The fundamental approach now widely used relies on equations in the form of the NLSE (10), and is based on the working assumption that modulational instability (MI) serves as an initial process in the formation of rogue waves. This hypothesis is also supported by numerical results.[47]

It has been recognized at an early stage that breather-type solutions of the NLSE may be good candidates for modeling of rogue waves.[48] Following their observation in nonlinear optics,[49–51] the first experimental observation of electrostatic rogue waves in plasmas was reported by Bailung.[52] A number of theoretical studies have since then focused on rogue waves in plasmas, e.g., in the contexts of Langmuir waves,[53] surface plasma waves,[54] dusty plasmas,[55] Alfvén waves,[56] electromagnetic beam-plasma interactions,[58] and more recently in dense (quantum) plasmas.[57,59]

In the following text, we shall summarize the current state of the art, as regards the basic analytical rogue wave-like solutions of the NLSE (10), briefly discussing their relevance in our physical model.

The *Peregrine soliton*[60] is now recognized as the fundamental candidate for rogue wave like behavior in physical systems modeled by the NLSE Eq. (10). Its relevance in nonlinear optics[50] and more recently in plasmas[52] has been established experimentally.

The Peregrine solution reads[58–60]

$$\psi = \exp iQt\left[1 - \frac{4(1+2iQt)}{1+\frac{2Q}{P}x^2+4Q^2t^2}\right]. \tag{15}$$

This solution has the form of a single-peaked structure that decays to a plane wave asymptotic background at either large x or t, but exhibits non-trivial behavior over a small region in (x, t), see Figure 4(a). For purposes of parametric analysis, all the pertinent physical information is contained within the coefficients P and Q in (15) which are functions of relevant plasma parameters; cf. (10) earlier.

The *Akhmediev breather* is given by[48,58,59]

$$\psi = \exp iQt \times \frac{\cosh(Q\sin(2\varphi)t - 2i\varphi) - \cos(\varphi)\cos\left(2\sin(\varphi)\sqrt{\frac{Q}{2P}}x\right)}{\cosh(Q\sin(2\varphi)t) - \cos(\varphi)\cos\left(2\sin(\varphi)\sqrt{\frac{Q}{2P}}x\right)}. \tag{16}$$

This waveform, which is periodic in space, but highly localized in time, cf. Figure 4(b), was recently detected in optical fibers.[51] The Peregrine solution is recovered in the limit of infinite spatial period.

The *Kuznetsov-Ma breather*[58,59,61] is given by the expression

$$\psi = \exp iQt \times \frac{\cosh(Q\sinh(2\varphi)t - 2i\varphi) - \cosh(\varphi)\cosh\left(2\sinh(\varphi)\sqrt{\frac{Q}{2P}}x\right)}{\cos(Q\sinh(2\varphi)t) - \cosh(\varphi)\cosh\left(2\sinh(\varphi)\sqrt{\frac{Q}{2P}}x\right)}. \tag{17}$$

This waveform is localized in space, but periodic in time; cf. Figure 4(c). Interestingly, one can recover the Peregrine solution in the limit of infinite temporal period.[48]

We close Sec. VI by referring the interested reader to Refs. 58 and 59, where the various types of rogue-wave breather solutions of the NLSE (10) are briefly reviewed. It is clear upon inspection of the latter expressions that the various plasma parameters affect the characteristics of these solutions via the coefficients P and Q. However, we have here limited ourselves to providing the above solutions, along with the representative, Figure 4, for the reader's information. A more detailed investigation of the parametric dependence of these solutions (along the lines of Refs. 58 and 59) was, for reasons of brevity in presentation, left for future work.

VII. PARAMETRIC INVESTIGATION

It is instructive to mention here that all plots provided here are based on a set of parameter values representative of relativistic degenerate plasmas found in dense astrophysical objects such as in white dwarfs, etc., where the typical interior densities are $\rho \sim 10^6$ g/cm^{-3}.[4,6]

We shall now investigate the effect of various relevant system parameters (carrier wavenumber k; positron-to-ion density ratio α; electron relativistic degeneracy parameter η_{e0}; ion-temperature to electron Fermi temperature ratio g) on the angular frequency ω, group velocity, v_g, the dispersion coefficient, P, the nonlinear coefficient, Q, the modulational stability profile and on the dynamics of the localized excitations. Two different regions of interest will be considered, as regards the parameter α (positron concentration). First, for very small α ($\ll 1$) (few or no positrons), the proposed model represents electron-ion (e-i) plasma at the first stages of positron production. On the other hand, for values near unity ($\alpha \simeq 1$—no ions present), we recover an e-p plasma. Both regimes are considered in the parametric analysis provided below.

Before starting the parametric analysis, we note that even though the scaling introduced in the present model is convenient and physically transparent, it invalidates

comparison among different plots for various parameter values, since some of these parameters can influence the scales. The functional dependence of the scales on the density is clearly identified through the dimensionless parameters α and η_{e0}. For the sake of clarity, we present the majority of the plots according to a scale which does not depend on these two parameters (see Figures 1–3 and 5–7), as explained in the end of Sec. II above.

Figure 4 is for illustration only. The scales used in the plots correspond to the fully dimensional representation, but scaled by certain constants which do not affect the figures in a qualitative manner. It should also be noted that when g $(\propto T_i/\eta_{e0}^2)$ is changed, we assume here that η_{e0} is held constant and T_i varies accordingly. Conversely, when η_{e0} varies for constant g, we assume that T_i changes to maintain the constant value of g. This was a matter of choice, for ease of representation and physical interpretation.

In Figures 1(a) and 1(b), we see that the frequency ω (in units of $\omega_0 = 8\pi(m_e^3c^3/6m_ih^3)^{1/2}$) increases as the wavenumber k (in units of $k_0 = 8\pi m_e e(c/3h^3)^{1/2}$) increases, as expected for an acoustic mode. On the other hand, ω (for given k, say) decreases as α acquires larger values. In Figure 1(c), we see that ω increases for higher values of η_{e0}. Recall that η_{e0} measures the relativistic character of the light constituents, hence small values of η_{e0} correspond to a "weakly-relativistic" regime, while higher values of η_{e0}, on the other hand, suggest a strongly relativistic behavior. Furthermore, Figure 1(d) shows that ω increases as g increases, an effect which is evident at higher values of k (shorter wavelength). Similar qualitative conclusions are drawn for the behavior of the group velocity v_g, depicted in Figure 2.

In order to investigate the envelope stability profile, let us recall that a key quantity is the ratio Q/P: its sign (positive/negative) corresponds to parameter regions of instability/stability, respectively), and determines the nature of envelope solitons to occur (bright/dark, respectively). The rogue wave-like breather solutions also occur in the "bright" region $(Q/P > 0)$.

We have studied the analytical behavior of the ratio Q/P (in units of $8k_0^2/m_e^2c^4$) versus the wavenumber k (in units of k_0), for different relevant plasma parameter values. In a general manner, $Q/P < 0$ for small k, suggesting stability for long wavelengths, as physically expected. For wavenumber values above a certain threshold, defined as the critical value k_c (i.e., essentially a root of either P or Q, since both are continuous analytical functions of k), Q/P becomes positive, suggesting that instability sets in above k_c.

The variation of Q/P with the wavenumber k for different values of the parameter η_{e0} is shown in Figure 5. The critical wavenumber k_c has a value $\simeq 1.3$ for $\eta_{e0} = 0.5$, reaching higher values for higher η_{e0} (viz., $k_c \simeq 1.9$ for $\eta_{e0} = 1$; $k_c \simeq 3.1$ for $\eta_{e0} = 2$). Dark envelope solitons therefore exist for values below the threshold k_c, while bright envelope solitons will occur above that value. In the modulationally stable region $k < k_c$ (see Figure 5(a)), the ratio $|Q/P|$ increases (in absolute value) with increasing η_{e0} for fixed value of k, suggesting wider (spatially extended) dark envelope-type solitons. In the modulationally unstable region $(k > k_c)$, the inverse behavior is observed, i.e., the ratio Q/P is reduced as η_{e0} increases, for given value of k, hence implying narrower bright-type envelope solitons for stronger relativistic regimes.

The dependence of the ratio Q/P on k for various values of the positron concentration α has been depicted in two cases of interest: (i) for low values of α and in (ii) for values

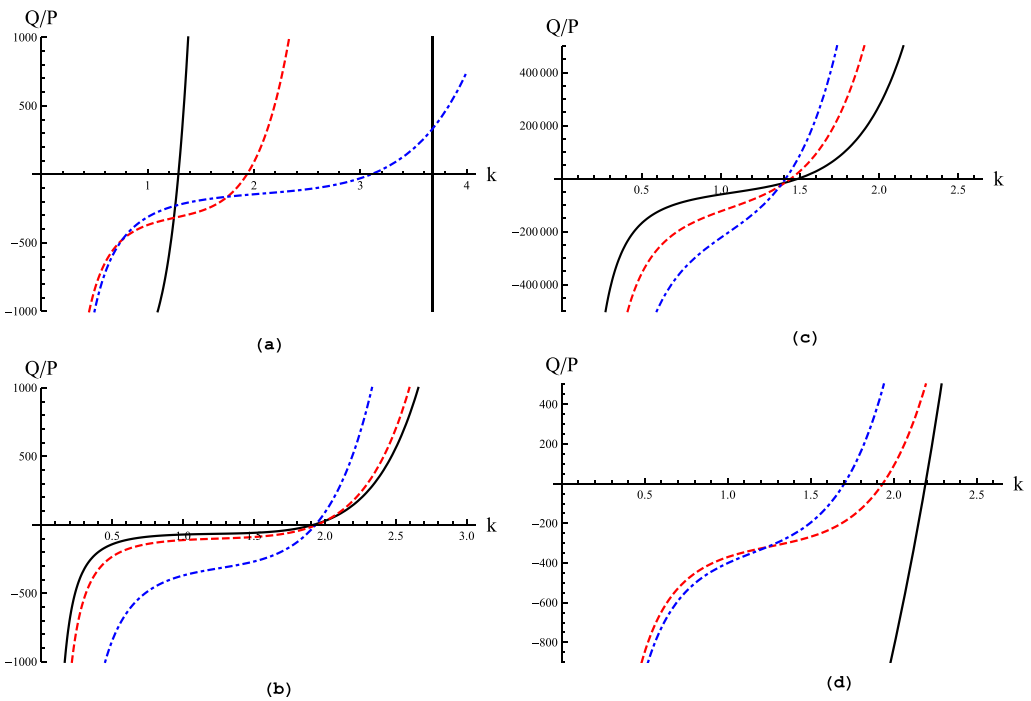

FIG. 5. The ratio Q/P (in units of $4k_0^2/m_e^2c^4$) is plotted against k (in units of k_0). In (a), $\alpha = 0.5$, $g = 0.01$; and the solid/dashed/dotted-dashed curves represent $\eta_{e0} = 0.5/1/2$. In (b), $\eta_{e0} = 1$, $g = 0.01$; and the solid/dashed/dotted-dashed curves represent low values of $\alpha = 0.025/0.1/0.5$. In (c), $\eta_{e0} = 1$, $g = 0.01$; and the solid/dashed/dotted-dashed curves represent higher values of $\alpha = 9/12/15$. In (d), $\eta_{e0} = 1$ and $\alpha = 0.5$ and the solid/dashed/dotted-dashed curves represent $g = 0.05/0.01/0.001$.

of α near unity. We note that in both cases (i) and (ii) an increase in α (i.e., keeping η_{e0} and g fixed) results in higher Q/P in the stable region (characterized by $k < k_c$, or $Q/P < 0$) as well as in the unstable region ($k > k_c$, or $Q/P > 0$, as shown in Figures 5(b) and 5(c).

We have plotted the ratio Q/P versus k, for different values of the ion temperature to the electron Fermi temperature ratio g. It appears from Figure 5(d) that increasing the thermal effects of ions (as manifested through higher g values) leads to a vertical shift of the curve downwards (i.e., to higher $|Q/P|$, in the negative region). A similar qualitative behavior is observed in the positive region, i.e., the ratio Q/P increases as g increases.

The dependence of the critical wavenumber (threshold) k_c (in units of k_0) on the relevant parameters is depicted in Figure 6. From these figures, we see that there are two critical values of k_c, namely, k_{c1} and k_{c2}, where the instability sets in. The critical wavenumber k_{c1} corresponds to $Q = 0$

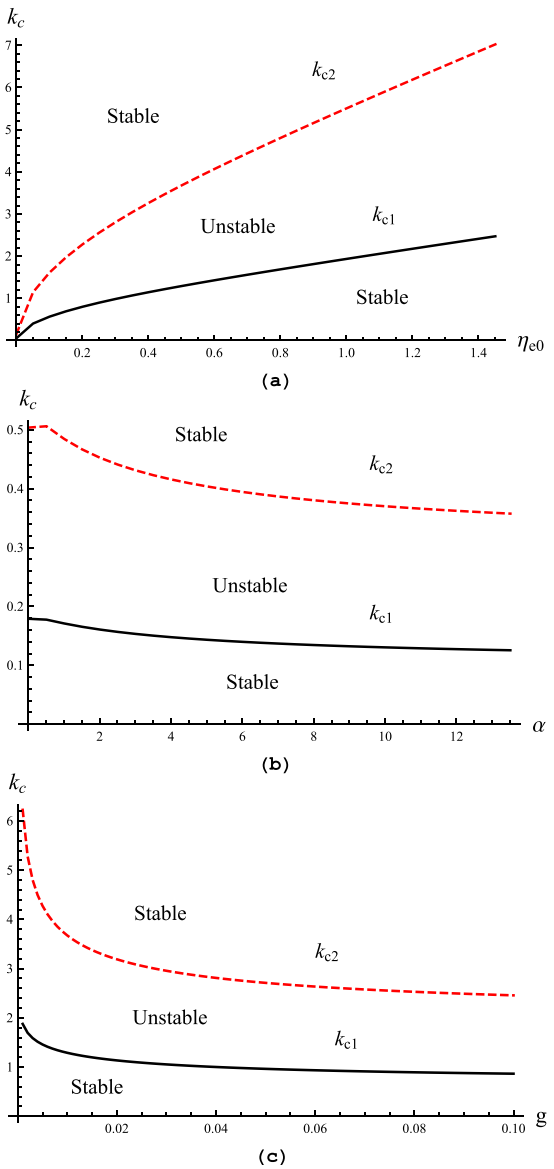

FIG. 6. The critical wavenumbers, k_{c1} and k_{c2} (both in units of k_0, are plotted in: (a) against η_{e0} with $\alpha = 0.5$ and $g = 0.01$; (b) against $\alpha = 0.5$ with $\eta_{e0} = g = 0.01$; (c) against g with $\alpha = \eta_{e0} = 0.5$.

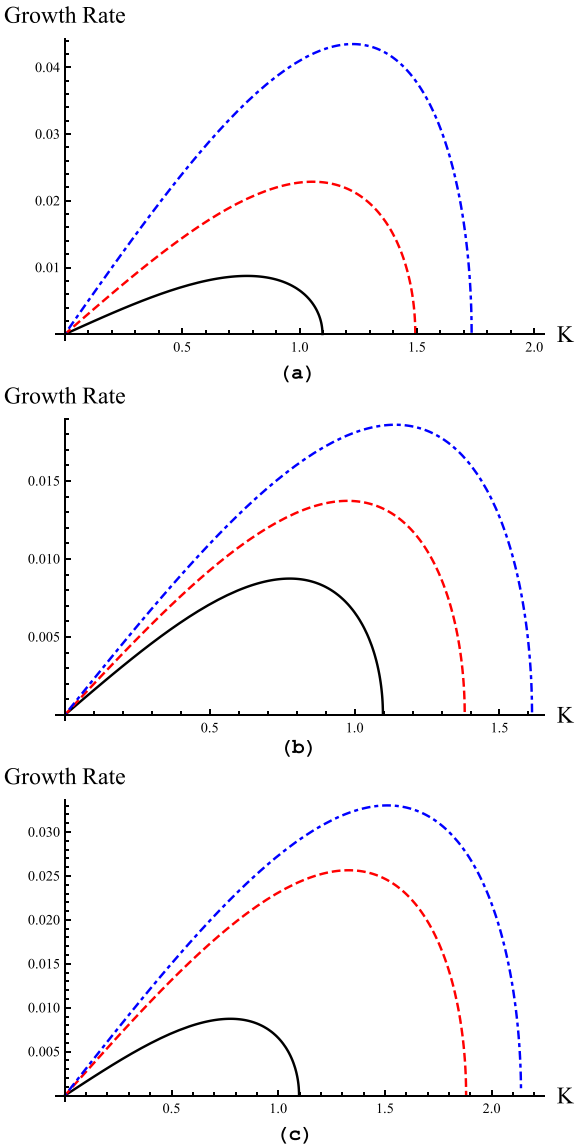

FIG. 7. The growth rate (in units of ω_0) is plotted against the perturbation wavenumber K ($\equiv \hat{k}$, in units of k_0). The value of the original dimensionless k is $k = 2.2$ in all cases. Note that the solid black curve is plotted for the same physical parameters in all the three panels for comparison; for $\alpha = 0.5$ and $\eta_{e0} = 5g = 0.05$. In (a), with $\alpha = 0.5$ and $g = 0.01$, the red dashed curve is for $\eta_{e0} = 0.1$ and the dotted-dashed blue curve is for $\eta_{e0} = 0.2$. In (b), with $\eta_{e0} = 5g = 0.05$, the red dashed curve is for $\alpha = 0.475$ and the dotted-dashed blue curve is for $\alpha = 0.45$. In (c), with $\alpha = 0.5$ and $\eta_{e0} = 0.05$, the red dashed curve is for $g = 0.0105$ and the dotted-dashed blue curve is for $g = 0.011$, respectively.

while k_{c2} to $P = 0$. In other words, these values correspond, respectively, to the ratio Q/P equal to zero or going to infinity. For wavenumbers lying in between the two critical values, $k_{c1} < k_c < k_{c2}$, the wave is unstable, while it is stable otherwise. The variation of k_c as a function of η_{e0} is shown in Figure 6(a). It is obvious that the unstable region is narrower for lower values of η_{e0}, while higher values of η_{e0} favors an increase in the modulationally unstable region. Figure 6(b) depicts the effect of the positron concentration α on the critical wavenumber k_c. Here it is seen that the curve of k_c appears to move downwards, i.e., the unstable region diminishes with increasing values of α. The same qualitative behavior of k_c is observed for increasing values of g (see

Figure 6(c) as was noticed in Figure 6(b)), i.e., increasing values of g results in the mitigation of unstable region.

Two comments are in order, regarding the instability threshold(s) depicted in Fig. 6. First, the upper curve in all subpanels of Fig. 6 is irrelevant in the cold-ion model, i.e., in the case $g=0$, it disappears (or, say, moves to infinity). Second, it is known that Landau damping (rather, its quantum analogue here[62,63]) occurs for wavenumber values in the vicinity of one (in reduced units), a fact which apparently invalidates quantitative results obtained for higher k, i.e., for short wavelengths. Indeed, beyond $k \simeq 1$, the fluid description may be inappropriate, as resonant particles are expected to interact and exchange energy with the wave,[62,63] a fact overlooked in the fluid description. The graphical analysis presented herewith is nonetheless provided for an extended parameter region, yet on an indicative (and qualitative) only basis, and should be read with some caution, if quantitative predictions are aimed at.

To obtain more information regarding the nature of modulational instability, we have displayed the growth rate (in units of ω_0) as a function of K (in units of k_0) for varying the relevant plasma parameters. The effect of α on the MI growth rate is depicted in Figure 7(a) (choosing a representative wavenumber in the unstable region). It is clear that the MI growth rate is significantly affected by α. In fact, the MI growth rate appears to be reduced with increasing α; the instability is somehow attenuated by the positron concentration. Moreover, we also note that increasing values of η_{e0} and g leads to increase the MI growth rate, suggesting that the instability is enhanced by higher values of η_{e0} and g (see Figures 7(b)–7(c)).

VIII. CONCLUSION

We have investigated from first principles the amplitude modulation of electrostatic wavepackets propagating in a completely degenerate dense plasma, which is composed of non-degenerate warm ions and relativistically degenerate electrons and positrons. A relativistic equation of state was employed for the electrons and positrons, while the ions were assumed to be an inertial species. By adopting a multiscale perturbation technique, a nonlinear Schrodinger equation was derived for the slow dynamics of the electrostatic wave envelope. Exact expressions for the dispersion (P) and nonlinearity (Q) coefficients were derived and their parametric dependence on the relevant parameters, namely, accounting for relativistic, positron and ion-pressure effects (via η_{e0}, α and g, respectively) was investigated.

We have shown that increasing values of η_{e0} would lead to an increase in k_c. On the other hand, increasing the value of α and g results in diminishing k_c, suggesting that modulational instability sets in for lower k.

The instability growth rate was found to decrease for higher values of α, concluding that increasing the positron concentration may somehow control the occurrence of MI. However, it was noticed that increasing the value of η_{e0} and g enhances the instability growth rate.

Furthermore, it was shown that increasing values of η_{e0} results in narrower bright-type envelope solitons (under constant amplitude), while, on the other hand, higher values of α and g give wider bright-type envelope excitations.

It may be added, for the sake of rigor, that we have adopted a semirelativistic fluid model, combining a classical algebraic operator structure with the Chandrasekhar pressure term[1] (in fact derived in a spherical geometry). It is thus understood that our model is valid for mildly relativistic regimes and for (1D linear) wave propagation in a 3D plasma geometry. A more elaborate model for strictly speaking 1D systems is in fact currently being elaborated,[64] and will be the subject of future work.

From a methodological point of view, our study relied on a straightforward application of the multiscale formalism introduced by Taniuti and coworkers [see Refs. 27 and 28]. This is a well established methodology in the multiscale description of spatially extended dynamical systems, which provides different options for different wavenumber k values (regions). It may be appropriate to compare our approach with (and distinguish it from) an alternative analytical approach, adopted, e.g., in Ref. 65, which essentially provides a long wavelength approximation of the relevant algebraic expressions. We note in particular, that the procedure adopted in the latter reference leads to coefficients P and Q (in our notation above) of opposite sign ($PQ<0$), hence only dark-type envelope solitons (and no, e.g., freak wave solutions nor bright envelope solitons)[58–60] in that limit.

It may be added for the sake of rigor that the positron production during laser-plasma interaction techniques appear to be a challenging topic recently, as ultraintense ultrashort laser pulses are made available via sophisticated technology, which gives rise to high density plasma entering the quantum regime.[19,66–68] Although admittedly at a somewhat speculative stage, we anticipate that our theoretical results will be relevant with fundamental electrostatic oscillations observed during those experiments.

ACKNOWLEDGMENTS

A.u.R. warmly acknowledges the financial support from the Higher Education Commission (HEC) of Pakistan under the International Research Support Initiative Program (IRSIP), in the form of a research fellowship held at Queen's University Belfast. I.K. and M.M.K. acknowledge the support from the FP7-PEOPLE-2013-IRSES Programme (Grant No. 612506 QUANTUM PLASMAS). I.K. gratefully acknowledges the support from the Brazilian research fund CNPq (Conselho Nacional de Desenvolvimento Científico e Tecnológico—Brasil).

APPENDIX: HARMONIC AMPLITUDE CONTRIBUTIONS

The solution in first order ($\sim\epsilon^1$) reads

$$n \approx \epsilon\, n_{i1}\, e^{i(kX_0-\omega T_0)} + \epsilon^2\left(\frac{1}{2}C_{2_1}^0|\psi|^2 + C_{2_1}^2\psi^2 e^{2i(kX_0-\omega T_0)}\right) + c.c.,$$

$$u \approx \epsilon n_1 e^{i(kX_0-\omega T_0)} + \epsilon^2\left(\frac{1}{2}C^0_{2_2}|\psi|^2 + C^2_{2_2}\psi^2 e^{2i(kX_0-\omega T_0)}\right) + c.c.$$

together with (9) for the electrostatic potential. Here we have omitted the first-harmonic contribution of the second order ($\sim\epsilon^2$) equations (physically amounting to a small addition to the dominant first harmonic). The lengthy expressions for the coefficients $C^l_{2_j}$ (for $l=0,\ 1,\ 2$ and $j=1,\ 2,\ 3$) are provided in the Appendix.

The coefficients C^0_{2l} (for $l=1,\ 2,\ 3$) are associated with the second-order, zeroth-harmonic components of the ion-density, speed and potential, respectively,

$$\begin{aligned} C^0_{2_1} &= \frac{c_1(c_1+k^2)^2\left(\frac{2v_g\omega}{k}+g+\frac{\omega^2}{k^2}\right)-2c_2}{c_1v_g^2-1-c_1g}, \\ C^0_{2_2} &= v_gC^0_{2_1} - 2\left(c_1+k^2\right)^2\frac{\omega}{k}, \\ C^0_{2_3} &= \frac{1}{c_1}C^0_{2_1} - \frac{2c_2}{c_1}. \end{aligned} \tag{A1}$$

The coefficients for the first-harmonic amplitudes at second order in ϵ are listed below

$$\begin{aligned} \phi^{(1)}_2 &= C^1_{2_3}\frac{\partial\psi}{\partial X_1} = 0, \\ n^{(1)}_2 &= C^1_{2_1}\frac{\partial\psi}{\partial X_1} = -2ik\frac{\partial\psi}{\partial X_1}, \\ v^{(1)}_2 &= C^1_{2_2}\frac{\partial\psi}{\partial X_1} = -i\omega\frac{\partial\psi}{\partial X_1}. \end{aligned} \tag{A2}$$

The coefficients C^2_{2l} (for $l=1,\ 2,\ 3$) are associated with the second-order, second-harmonic components

$$\begin{aligned} C^2_{2_1} &= \left(c_1+4k^2\right)C^2_{2_3}+c_2, \\ C^2_{2_2} &= \frac{\omega}{k}C^2_{2_1} - \left(c_1+k^2\right)^2\frac{\omega}{k}, \\ C^2_{2_3} &= \frac{\frac{(c_1+k^2)^2}{2}\left(3\omega^2+gk^2\right)-c_2\left(\omega^2-gk^2\right)}{3k^2\left(\omega^2-gk^2\right)}. \end{aligned} \tag{A3}$$

In terms of the various coefficients appearing in the latter expression have been defined above, the nonlinearity coefficient Q in Eq. (10) is given by

$$Q = \frac{\left(\omega^2-gk^2\right)\left[2c_2\left(C^0_{2_3}+C^2_{2_3}\right)+3c_3\right]}{2\omega(c_1+k^2)} - k\left(C^0_{2_2}+C^2_{2_2}\right) - \frac{\left(\omega^2+gk^2\right)\left(C^0_{2_1}+C^2_{2_1}\right)}{2\omega}. \tag{A4}$$

[1]S. Chandrasekhar, *An Introduction to the Study of Stellar Structure* (The University of Chicago Press, Chicago, 1939).
[2]A. Y. Potekhin, D. A. Baiko, P. Haensel, and D. G. Yakovlev, Astron. Astrophys. **346**, 345 (1999).
[3]G. Chabrier, D. Saumon, and A. Y. Potekhin, J. Phys. A: Math. Gen. **39**, 4411 (2006).
[4]D. Koester and G. Chanmugam, Rep. Prog. Phys. **53**, 837 (1990).
[5]S. H. Glenzer and R. Redmer, Rev. Mod. Phys. **81**, 1625 (2009).
[6]S. L. Shapiro and S. A. Teukolsky, *Black Holes, White Dwarfs, and Neutron Stars: The Physics of Compact Objects* (Wiley, New York, 1983).
[7]S. Chandrasekhar, Mon. Not. R. Astron. Soc. **170**, 405 (1935).
[8]A. A. Mamun and P. K. Shukla, Phys. Plasmas **17**, 104504 (2010).
[9]I. Zeba, W. M. Moslem, and P. K. Shukla, Astrophys. J. **750**, 72 (2012).
[10]M. Akbari-Moghanjoughi, Astrophys. Space Sci. **332**, 187 (2011).
[11]F. C. Michel, Rev. Mod. Phys. **54**, 1 (1982).
[12]F. C. Michel, *Theory of Neutron Star Magnetosphere* (Chicago University Press, Chicago, 1991).
[13]H. R. Miller and P. J. Witta, *Active Galetic Nuclei* (Springer-Verlag, Berlin, 1987), p. 202.
[14]M. L. Burns, *Positron-Electron Pairs in Astrophysics*, edited by M. L. Burns, A. K. Harding, and R. Ramaty (American Institute of Physics, Melville, NY, 1983).
[15]K. Kashiyama, K. Ioka, and N. Kawanaka, Phys. Rev. D **83**, 023002 (2011).
[16]M. J. Rees, *The Very Early Universe* (Cambridge University Press, Cambridge, 1983), p. 275.
[17]C. M. Surko and T. Murphy, Phys. Fluids B **2**, 1372 (1990).
[18]C. P. Ridgers, C. S. Brady, R. Duclous, J. G. Kirk, K. Bennett, T. D. Arber, A. P. L. Robinson, and A. R. Bell, Phys. Rev. Lett. **108**, 165006 (2012).
[19]G. Sarri, W. Schumaker, A. Di. Piazza, K. Poder, J. M. Cole, M. Vargas, D. Doria, S. Kushel, B. Dromey, G. Grittani, L. Gizzi, M. E. Dieckmann, A. Green, V. Chvykov, A. Maksimchuk, V. Yanovsky, Z. H. He, B. X. Hou, J. A. Nees, S. Kar, Z. Najmudin, A. G. R. Thomas, C. H. Keitel, K. Krushelnick, and M. Zepf, Plasma Phys. Controlled Fusion **55**, 124017 (2013).
[20]R. Lallement, B. Y. Welsh, M. A. Barstow, and S. L. Casewell, Astron. Astrophys. **533**, A140 (2011).
[21]R. Svensson, Astrophys. J. **258**, 335 (1982).
[22]A. Esfandyari-Kalejahi, I. Kourakis, M. Mehdipoor, and P. K. Shukla, J. Phys. A: Math. Gen. **39**, 13817 (2006).
[23]M. Akbari-Moghanjoughi, Phys. Plasmas **18**, 012701 (2011).
[24]A. Rahman, S. Ali, A. Mushtaq, and A. Qamar, J. Plasma Phys. **79**, 817 (2013).
[25]S. A. Khan, Astrophys. Space Sci. **343**, 683 (2013).
[26]G. Williams and I. Kourakis, Phys. Plasmas **20**, 122311 (2013).
[27]T. Taniuti and N. Yajima J. Math. Phys. **10**, 1369 (1969).
[28]N. Asano, T. Taniuti, and N. Yajima, J. Math. Phys. **10**, 2020 (1969).
[29]S. Watanabe, J. Plasma Phys. **17**, 487 (1977).
[30]X. Jukui and T. Rongan, Phys. Scr. **67**, 74 (2003).
[31]I. Kourakis and P. K. Shukla, Eur. Phys. J. D **28**, 109 (2004).
[32]I. Kourakis and P. K. Shukla, Phys. Scr. **69**, 316 (2004).
[33]I. Kourakis and P. K. Shukla, Nonlinear Processes Geophys. **12**, 407 (2005).
[34]W. F. El-Taibany and I. Kourakis, Phys. Plasmas **13**, 062302 (2006).
[35]W. F. El-Taibany, I. Kourakis, and M. Wadati, Plasma Phys. Controlled Fusion **50**, 074003 (2008).
[36]R. Tang and J. Xue, Phys. Plasmas **11**, 3939 (2004).
[37]T. S. Gill, C. Bedi, and A. S. Bains, Phys. Scr. **81**, 055503 (2010).
[38]M. Remoissenet, *Waves Called Solitons* (Springer, Berlin, 1996); T. Dauxois and M. Peyrard, *Physics of Solitons* (Cambridge University Press, 2005).
[39]R. Fedele and H. Schamel, Eur. Phys. J. B **27**, 313 (2002).
[40]S. Sultana and I. Kourakis, Plasma Phys. Controlled Fusion **53**, 045003 (2011).
[41]I. Kourakis and P. K. Shukla, J. Phys. A: Math. Gen. **36**, 11901 (2003).
[42]R. Fedele, Phys. Scr. **65**, 502 (2002); R. Fedele, H. Schamel, and P. K. Shukla, *ibid.* **2002**, 18.
[43]C. Kharif, E. Pelinovsky, and A. Slunyaev, *Rogue Waves in the Ocean* (Springer, Heidelberg, 2009).
[44]A. Osborne, *Nonlinear Ocean Waves* (Academic Press, 2009).
[45]A. Ankiewicz, N. Devine, and N. Akhmediev, Phys. Lett. A **373**, 3997 (2009).
[46]P. K. Shukla, I. Kourakis, B. Eliasson, M. Marklund, and L. Stenflo, Phys. Rev. Lett. **97**, 094501 (2006).
[47]R. Peric, N. Hoffmann, and A. Chabchoub, "Initial wave breaking dynamics of Peregrine-type rogue waves: A numerical and experimental study" (2014), see http://arxiv.org/abs/1401.0949.
[48]K. B. Dysthe and K. Trulsen, Phys. Scr. **T82**, 48 (1999).
[49]D. R. Solli, C. Ropers, P. Koonath, and B. Jalali, Nature **450**, 1054 (2007).

[50]B. Kibler, J. Fatome, C. Finot, G. Millot, F. Dias, G. Genty, N. Akhmediev, and J. M. Dudley, Nat. Phys. A **6**, 790 (2010).
[51]B. Kibler, J. Fatome, C. Finot, G. Millot, G. Genty, B. Wetzel, N. Akhmediev, F. Dias, and J. M. Dudley, Sci. Rep. **2**, 463 (2012).
[52]H. Bailung, S. K. Sharma, and Y. Nakamura, Phys. Rev. Lett. **107**, 255005 (2011).
[53]W. M. Moslem, Phys. Plasmas **18**, 032301 (2011).
[54]W. M. Moslem, P. K. Shukla, and B. Eliasson, EPL **96**, 25002 (2011).
[55]W. M. Moslem, R. Sabry, S. K. El-Labany, and P. K. Shukla, Phys. Rev. E **84**, 066402 (2011).
[56]P. K. Shukla and W. M. Moslem, Phys. Lett. A **376**, 1125 (2012).
[57]R. Sabry, W. M. Moslem, and P. K. Shukla, Phys. Plasmas **19**, 122903 (2012).
[58]G. P. Veldes, J. Borhanian, M. McKerr, V. Saxena, D. J. Frantzeskakis, and I. Kourakis, J. Opt. **15**(Special Issue), 064003 (2013).
[59]M. McKerr, I. Kourakis, and F. Haas, Plasma Phys. Controlled Fusion **56**, 035007 (2014).
[60]D. H. Peregrine, J. Aust. Math. Soc., Ser. B **25**, 16 (1983).
[61]E. A. Kuznetsov, Dokl. Akad. Nauk SSSR **236**, 575 (1977); E. A. Kuznetsov, Sov. Phys. Dokl. **22**, 507 (1977) (Engl. transl.).
[62]F. Haas, *Quantum Plasmas—An Hydrodynamic Approach* (Springer, New York, 2011).
[63]G. Manfredi, Fields Inst. Commun. **46**, 263 (2005).
[64]F. Haas and I. Kourakis, in Proceedings of the International Congress on Plasma Physics, Lisbon Portugal, 15–19 September, 2014.
[65]S. A. El-Tantawy and W. M. Moslem, Phys. Plasmas **21**, 052112 (2014).
[66]G. Sarri, W. Schumaker, A. Di Piazza, M. Vargas, B. Dromey, M. E. Dieckmann, V. Chvykov, A. Maksimchuk, V. Yanovsky, Z. H. He, B. X. Hou, J. A. Nees, A. G. R. Thomas, C. H. Keitel, M. Zepf, and K. Krushelnick, "Table-top laser-based source of femtosecond, collimated, ultrarelativistic positron beams," Phys. Rev. Lett. **110**, 255002 (2013).
[67]G. Sarri, K. Poder, J. Cole, W. Schumaker, A. Di Piazza, B. Reville, T. Dzelzainis, D. Doria, L. A. Gizzi, G. Grittani, S. Kar, H. Keitel, K. Krushelnick, S. Kuschel, S. P. D. Mangles, Z. Najmudin, N. Shukla, L. O. Silva, D. Symes, A. G. R. Thomas, M. Vargas, J. Vieira, and M. Zepf, "Generation of neutral and high-density electron-positron pair plasmas in the laboratory," Nat. Commun. (submitted).
[68]G. Sarri, M. Dieckmann, I. Kourakis, A. di Piazza, B. Reville, C. Keitel, and M. Zepf, "Laser-driven generation of electron-positron beams: A review," J. Plasma Phys. (submitted).